Journal of Molecular and Cellular Cardiology 181 (2023) 89–97

Contents lists available at ScienceDirect

Journal of Molecular and Cellular Cardiology

journal homepage: www.elsevier.com/locate/yjmcc

Top-down proteomics of myosin light chain isoforms define chamber-specific expression in the human heart

Elizabeth F. Bayne [a], Kalina J. Rossler [b,c], Zachery R. Gregorich [d], Timothy J. Aballo [b,c], David S. Roberts [a], Emily A. Chapman [a], Wei Guo [d], Sean P. Palecek [e], J. Carter Ralphe [f], Timothy J. Kamp [c,g], Ying Ge [a,b,c,h,*]

[a] Department of Chemistry, University of Wisconsin-Madison, Madison, WI 53706, USA
[b] Molecular and Cellular Pharmacology Training Program, University of Wisconsin-Madison, Madison, WI 53705, USA
[c] Department of Cell and Regenerative Biology, University of Wisconsin-Madison, Madison, WI 53705, USA
[d] Department of Animal and Dairy Sciences, University of Wisconsin-Madison, Madison, WI 53706, USA
[e] Department of Chemical and Biological Engineering, University of Wisconsin-Madison, Madison, WI 53706, USA
[f] Department of Pediatrics, University of Wisconsin–Madison, Madison, WI 53705, USA
[g] Department of Medicine, University of Wisconsin–Madison, Madison, WI 53705, USA
[h] Human Proteomics Program, School of Medicine and Public Health, University of Wisconsin-Madison, Madison, WI 53705, USA

ARTICLE INFO

Keywords:
Mass spectrometry
Top-down proteomics
Sarcomere proteins
Myosin light chains
Human hearts
PTMs

ABSTRACT

Myosin functions as the "molecular motor" of the sarcomere and generates the contractile force necessary for cardiac muscle contraction. Myosin light chains 1 and 2 (MLC-1 and -2) play important functional roles in regulating the structure of the hexameric myosin molecule. Each of these light chains has an 'atrial' and 'ventricular' isoform, so called because they are believed to exhibit chamber-restricted expression in the heart. However, recently the chamber-specific expression of MLC isoforms in the human heart has been questioned. Herein, we analyzed the expression of MLC-1 and -2 atrial and ventricular isoforms in each of the four cardiac chambers in adult non-failing donor hearts using top-down mass spectrometry (MS)-based proteomics. Strikingly, we detected an isoform thought to be ventricular, MLC-2v (gene: *MYL2*), in the atria and confirmed the protein sequence using tandem MS (MS/MS). For the first time, a putative deamidation post-translation modification (PTM) located on MLC-2v in atrial tissue was localized to amino acid N13. MLC-1v (*MYL3*) and MLC-2a (*MYL7*) were the only MLC isoforms exhibiting chamber-restricted expression patterns across all donor hearts. Importantly, our results unambiguously show that MLC-1v, not MLC-2v, is ventricle-specific in adult human hearts. Moreover, we found elevated MLC-2 phosphorylation in male hearts compared to female hearts across each cardiac chamber. Overall, top-down proteomics allowed an unbiased analysis of MLC isoform expression throughout the human heart, uncovering previously unexpected isoform expression patterns and PTMs.

1. Introduction

The hexameric protein complex myosin functions as the "molecular motor" of the sarcomere and generates contractile force through cross bridge formation with actin [1,2]. In cardiac tissue, myosin is composed of two heavy chains (MHC, either the α or β isoform) and four light chains (MLCs), which include two essential (ELC, or MLC-1) and two regulatory (RLC, or MLC-2) light chains [3–5]. MLC-1 provides structural stability whereas MLC-2 regulates the function of the myosin motor through calcium binding and phosphorylation [3]. MLC-1 and -2 each have two isoforms encoded by separate genes: *MYL4* and *MYL3* encode MLC-1a and MLC-1v, respectively, and *MYL7* and *MYL2* encode MLC-2a and MLC-2v [6,7].

Each respective light chain has an 'atrial' and a 'ventricular' isoform so called because early studies suggested the expression of these isoforms in the heart is chamber specific [8,9]. It is noteworthy that MLC-2v has become a commonly-used marker of ventricular specification in stem cell-derived cardiomyocyte (hPSC-CM) cultures [10]. However, the initial analysis of MLC expression in the heart was performed in small animal models and thus, the findings may not directly translate to

* Corresponding author at: 1111 Highland Ave., WIMR II 8551, Madison, WI 53705, USA.
E-mail address: ying.ge@wisc.edu (Y. Ge).

https://doi.org/10.1016/j.yjmcc.2023.06.003
Received 28 January 2023; Received in revised form 27 May 2023; Accepted 13 June 2023
Available online 14 June 2023

humans due to significant physiological differences between rodent and human hearts [11–14]. Larger animal models are preferred for modeling cardiovascular disease because they have been shown to better replicate human cardiac physiology compared to small animal models [15–19]. In particular, the myofilament composition and post-translational modifications (PTMs) of swine heart show greater similarity to humans than rodents [20–23]. Our previous study of the sarcomeric proteome in Yorkshire domestic pig hearts demonstrated the chamber-specific expression of MLC-1 and -2 ventricular and atrial isoforms [24]. Nevertheless, despite the high similarity, there are still differences between large animal and human hearts so that a direct interrogation of human samples is essential [25]. Thus, we performed a direct analysis of a sex-balanced cohort of non-failing human donor hearts to decipher basal levels of MLC isoform expression and PTMs across the four chambers of the human heart in both sexes.

Top-down proteomics analyzes intact proteins, enabling unbiased analysis of proteoforms, a term describing all protein products produced from a single gene as a result of post-translational modifications (PTMs), sequence variants, and alternative splicing [26], as well as related proteins arising from different genes (*e.g.*, isoforms not resulting from alternative splicing of a single gene) [27–31]. In contrast to the conventional bottom-up proteomics which analyzes peptides digested from proteins thus suffers from the peptide-to-protein inference problem [32,33], top-down proteomics analyzes proteins directly without digestions, providing accurate identification and quantification of protein isoforms and PTMs [27–29,34]. Thus, a direct analysis of MLC isoforms and proteoforms by top-down proteomics allows accurate quantification of their levels without *a priori* knowledge of sample contents. Previously, top-down proteomics was employed to characterize the amino acid sequences and N-terminal modifications of atrial and ventricular MLC isoforms from human and swine myocardial tissue [35].

In this study, we employed top-down mass spectrometry (MS)-based proteomics to systematically evaluate differences in MLC proteoform and isoform expression in the four chambers of non-failing human donor hearts (n = 17). Surprisingly, our analysis revealed MLC-1v, but not MLC-2v, exhibited ventricle-specific expression, while MLC-2a exhibits atria-restricted expression. The exact amino acid sequence of MLC-2v in atrial tissue was then confirmed by online liquid chromatography-tandem MS (LC-MS/MS). Interestingly, we found a mixture of deamidated and non-deamidated MLC-2v species in the atria that was not observed in ventricular tissue. Overall, top-down proteomics provided us with an unbiased analysis of the MLC proteoform distribution in the four chambers of the non-failing adult human heart.

2. Materials and methods

2.1. Human donor heart collection

Myocardial tissue from adult donor hearts with no history of cardiovascular disease were obtained from the University of Wisconsin Organ Procurement Organization (Table S1 details clinical characteristics). Tissue collection procedures were approved by the Institutional Review Board of the University of Wisconsin-Madison (Study # 2013–1264). Cardiac tissue was dissected into left ventricle (LV), right ventricle (RV), left atrium (LA), and right atrium (RA) while fresh and immediately snap frozen in liquid nitrogen to preserve PTMs [36] (Fig. S1). The basal ventricular mid-wall was used as a representative region for LV and RV.

2.2. Sarcomeric protein extraction

Sarcomeric proteins were extracted from human cardiac tissue using differential pH extraction as reported previously (Fig. S2) [36,37]. Cardiac tissue was homogenized in 10 volumes of a pH-neutral buffer (25 mM HEPES pH 7.4, 60 mM NaF, 1 mM Na3VO4, 1 mM PMSF, 2.5 mM EDTA, and 1× Halt Protease and Phosphatase inhibitor) and centrifuged for 30 min at 18,000 ×g at 4 °C. The supernatant was removed, and the remaining pellet was homogenized in a 1% TFA solution (1% TFA, 1 mM TCEP, 10 mM L-Methionine) and centrifuged at 21,000 ×g at 4 °C for 15 min. The resulting myofilament-enriched supernatant ("TFA extract") was prepared for MS analysis. The total protein content of the TFA extract was normalized by biochitonic assay and prepared in a diluent of 0.1% formic acid at 2 mM TCEP. Proteins were separated by online reversed phase liquid chromatography (LC) prior to MS analysis (LC-MS).

2.3. Online LC-MS analysis

LC-MS profiling was performed using a NanoAcquity ultra-high pressure LC system (Waters, Milford, MA) coupled to a high-resolution impact II quadrupole time-of-flight (Q-TOF) mass spectrometer (Bruker, Bremen, Germany) [24,38]. 400 ng total protein per injection were loaded on a home-packed PLRP column (250 μm i.d. x 200 mm length, PLRP-S, 10 μm particle size, 1000 Å pore size). Sarcomeric proteins were eluted using a flow rate of 4 μL/min over a gradient of 5% to 95% mobile phase B (0.1% formic acid in 50:50 acetonitrile and ethanol) over 40 min (mobile phase A: 0.1% formic acid in water). Electrospray ionization was used to introduce eluted proteins to the impact II Q-TOF mass spectrometer. Mass spectra were acquired at a scan rate of 0.5 Hz over 500–2000 m/z range. Injection replicates (n = 3) were performed at the beginning of each run to ensure instrument reproducibility and extraction replicates (n = 3) were analyzed to evaluate the reproducibility of sample preparation. Isotopic resolution was achieved for each analyte, and all proteins were identified with high mass accuracy (<3 ppm mass error).

Online tandem mass spectra were collected by data-dependent acquisition settings. The top 5 highest intensity precursors were selected and fragmented using collision-induced dissociation (CID). MS1 scan rate was 1 Hz and MS2 scan rate varied from 4 to 8 Hz depending on precursor ion intensity. Collisional energies were set to 18–45 eV. An active exclusion period of 1 min was used to maximize number of precursors selected. Electron Transfer Dissociation (ETD) was performed on the maXis II Q-TOF MS. The top 3 most abundant precursors in each MS1 spectrum were selected for fragmentation. The ETD settings were as follows: ion charge control ranging from 0 to 1000 ms, a reagent accumulation time of 25 ms, and an extended reaction time of 50 ms.

2.4. Data analysis

Mass spectra were analyzed using DataAnalysis v4.3 (Bruker Daltonics) and MASH Explorer [39]. Mass spectra were averaged across retention time windows within the BPC to create MS1 spectra. Spectral deconvolution using the Maximum Entropy algorithm with a resolving power of 60,000 was performed to reveal the monoisotopic mass of the protein, and putative proteoform identifications are made based on accurate mass. Peaks whose molecular masses matched closely to predicted masses from the UniProtKB database (≤ 10 ppm mass error) were assigned the corresponding proteoform identity (Table S2). Phosphorylated proteoform quantitation is performed using peak intensities of unmodified and phosphorylated peaks, yielding a ratio of relative phosphorylation, P_{total} (mol P_i/mol protein), reported as average ± Standard Error of the Mean (SEM) [22]. [40] Theoretical isotopic distributions of precursor and fragment ions were generated using IsoPro v3.0.

To better visualize isoforms over a wide retention time window, extracted ion chromatograms (EICs) were generated for quantitation (Fig. S3). To quantitate relative intensities of isoforms in each sample, peak intensities from deconvoluted spectra were used if the isoforms eluted within the selected retention time window. To quantitate the relative intensity of isoforms in each sample, EICs were created from the top 5 most abundant ions (± 0.2 m/z) for each proteoform as described previously [41]. Isoform intensity was normalized by dividing the peak

areas under the curve (AUC) by the sum of peak areas for all isoforms pertaining to the protein family (*e.g.* MLC-1v/total MLC-1 content) [38]. For tandem MS sequence characterization, the monoisotopic mass of each fragment ion was analyzed against each putative protein sequence using IsoPro v3.0 using a mass error tolerance of 10 ppm. Isotopic distributions and theoretical fit were generated using IsoPro.

2.5. Statistics

P_{total} values were analyzed for statistical significance using RStudio v1.2.5033. Differences between four chambers were evaluated using a linear model. One-way analysis of variance (ANOVA) was used to determine statistical significance between the four chambers. Tukey's HSD *post hoc* test was used for a pairwise evaluation between regions and adjusted p values are reported. A 95% confidence interval was used for Tukey's HSD. Differences between means were considered statistically significant if $p < 0.05$. Levels of statistical significance are notated with an asterisk (*): $*p \leq 0.05$, $**p < 0.01$, and $***p < 0.001$; no statistical significance *(ns)* if $p > 0.05$.

3. Results

In this study, we employed top-down MS-based proteomics to comprehensively analyze the expression patterns of MLC-1 and -2 isoforms across the four chambers of non-failing human donor hearts ($n = 17$). Clinical characteristics of donors used in this study are presented in Table S1. Our platform efficiently captures the diversity of a complex protein mixture, enabling quantification of the relative abundance of proteoforms and isoforms in a single LC-MS experiment. This approach includes myocardial tissue homogenization, sarcomeric protein extraction, LC-MS/MS, and data analysis (Fig. S2).

3.1. Myofilament protein extraction and LC-MS/MS platform is highly reproducible

Technical reproducibility of the online LC-MS/MS platform was demonstrated by alignment of retention times and intensity of base peak chromatograms (BPC) between injections (Fig. S4). Method reproducibility was established by replicate extraction of proteins from the same cardiac chamber ($n = 3$) (Fig. S5). Proteoform quantitation was demonstrated by comparable intensity of the phosphorylated MLC-2v proteoform between extraction replicates (Fig. S5B). Reproducible isoform quantitation was demonstrated by comparing the integrated area of MLC-2v EICs between technical replicates, ranging from 0.1 to 6% relative standard deviation across each cardiac chamber (Fig. S5C). Finally, we demonstrated the highly reproducible detection of MLC-2v proteoform in atrial tissue despite the fact that the extraction and LC-MS sample runs were performed by different personnel (Fig. S6). MS-based quantification of MLC expression was performed confidently after demonstration of high technical and extraction reproducibility.

3.2. Top-down MS and MS/MS analysis of MLC-1 shows MLC-1v is chamber-specific

MLC-1a and MLC-1v were detected with high mass accuracy, matching their respective theoretical monoisotopic masses with high mass accuracy (Fig. 1A, Table S2). MS analysis revealed single peaks corresponding to the ventricular and atrial MLC-1 isoforms in their respective chambers. The peak with a molecular mass of 21,828.91 Da detected in ventricular tissue matched well with the MLC-1v sequence in the UniProt/SwissProt database (Accession No. P08590–1, MYL3_HUMAN) when considering N-terminal methionine removal (−131.04 Da) and N^{α}-trimethylation (+42.05 Da), consistent with previous reported N-terminal modifications (theoretical mass: 21,828.93 Da, 0.9 ppm mass error) [35]. The peak detected in atrial tissue with a molecular mass of 21,461.79 Da matched with the reported sequence of MLC-1a (Accession No. P12829–1, MYL4_HUMAN) when accounting for N-terminal methionine removal and N^{α}-trimethylation as reported previously (theoretical mass: 21,461.87 Da, 3 ppm mass error) [35].

LC-MS/MS generated N- and C-terminal protein fragment ions using CID. Fragment ions confirmed the MLC-1 isoform sequences with N-terminal modifications as previously reported [35]. Ions corresponding to MLC-1v, including b_{23} and y_{80}, were observed consistently across LV and RV preparations from different hearts (Fig. S7A), matching closely to theoretical isotopic distributions with high mass accuracy. In total, 22 b and 16 y ions were identified within ≤10 ppm mass error, corresponding to 87% sequence coverage of MLC-1v from a single LC-MS/MS run (Fig. S8). Similarly, key N- and C-terminal fragments matching MLC-1a were identified with consistency across LA and RA preparations from different hearts, matching theoretical isotopic distributions with high mass accuracy (Fig. S7B). MLC-1a fragmentation by CID yielded 31 total b and 15 y ions within ≤10 ppm mass error (Fig. S9). Sequence alignment of MLC-1v and MLC-1v revealed 80.5% sequence similarity between isoforms (Fig. S10A).

Quantification of MLC-1 isoforms revealed MLC-1v was ventricle-specific. MLC-1v was the most abundant isoform in LV and RV, averaging 99 ± 0.6% MLC-1v in LV and 97 ± 1.1% in RV (Fig. 1C, Fig. S11). In-depth analysis of the raw mass spectra showed MLC-1v was not detected above baseline noise in LA and RA (Fig. S12). One-way ANOVA was used to evaluate MLC-1v expression across the four chambers ($p = 2.2e\text{-}16$), and pairwise comparisons revealed statistically significant contrasts between LA and RA when compared to LV and RV ($p < 0.0001$ for each comparison, for details refer to Table S3). No lateral distinctions were noted in the ventricles and atria (LV-RV $p = 0.27$; LA-RA $p = 1.00$).

3.3. Ventricular isoform of MLC-2 detected in atrial tissues using LC-MS/MS

Top-down MS revealed 2 proteoforms related to MLC-2v and 3 proteoforms related to MLC-2a. Two proteoforms with molecular masses of 18,699.40 and 18,768.36 Da were detected in each cardiac chamber (Fig. 1B, Table S2). The peak with a mass of 18,699.40 Da matched the calculated molecular mass of MLC-2v (Accession No. P10916–1, MLRV_HUMAN) with 3 ppm mass error after considering N-terminal methionine cleavage and N^{α}-trimethylation as previously reported. The peak of 18,768.36 Da was an additional +79.97 Da from MLC-2v, corresponding to the addition of meta-phosphoric acid HPO_3 and, thus, was assigned as mono-phosphorylated pMLC-2v (2 ppm mass error). The remaining three proteoforms were exclusively detected in atria and had molecular masses of 19,346.54, 19,426.50, and 19,506.47 Da. The 19,346.54 Da peak matches with predicted molecular mass of MLC-2a (Accession No. Q01449–1, MLRA_HUMAN) with 3 ppm mass error after considering N-terminal methionine cleavage and N^{α}-acetylation (+42.01 Da). Mono-phosphorylated $_p$MLC-2a was assigned to the peak of 19,426.50 Da due to an addition of +79.97 Da from MLC-2a (5 ppm mass error) and bis-phosphorylated $_p$MLC-2a was assigned to peak of 19,506.47 Da due to a mass difference of +159.91 Da (2 ppm mass error). Each isoform showed good fitting of theoretical isotopic abundance and distribution of the isotopomer peaks (Fig. S14), including phosphorylated proteoforms (Fig. S15).

MS/MS enabled by CID was used to confirm the identity of MLC-2v and pMLC-2v across the four cardiac chambers. A total of 47 MLC-2v fragment ions were identified across LV, RV, LA, and RA, including 22 b and 25 y ions (Fig. S16). For example, the y_{24} ion corresponding to C-terminal MLC-2v matched closely to the theoretical isotopic distribution for each cardiac chamber, and the experimentally determined mass matches the theoretical mass with sub-ppm accuracy, indicating agreement with previously reported MLC-2v sequence (Fig. S17A). Phosphorylation of MLC-2v was also confirmed by tandem MS (Fig. S18). 33 fragment ions were identified correlating to pMLC-2v, including 13 b and 20 y ions (Fig. S18B). Fragment ion spectra enabled the mapping of phosphorylation site to Ser14 by detecting N-terminal b ions before and

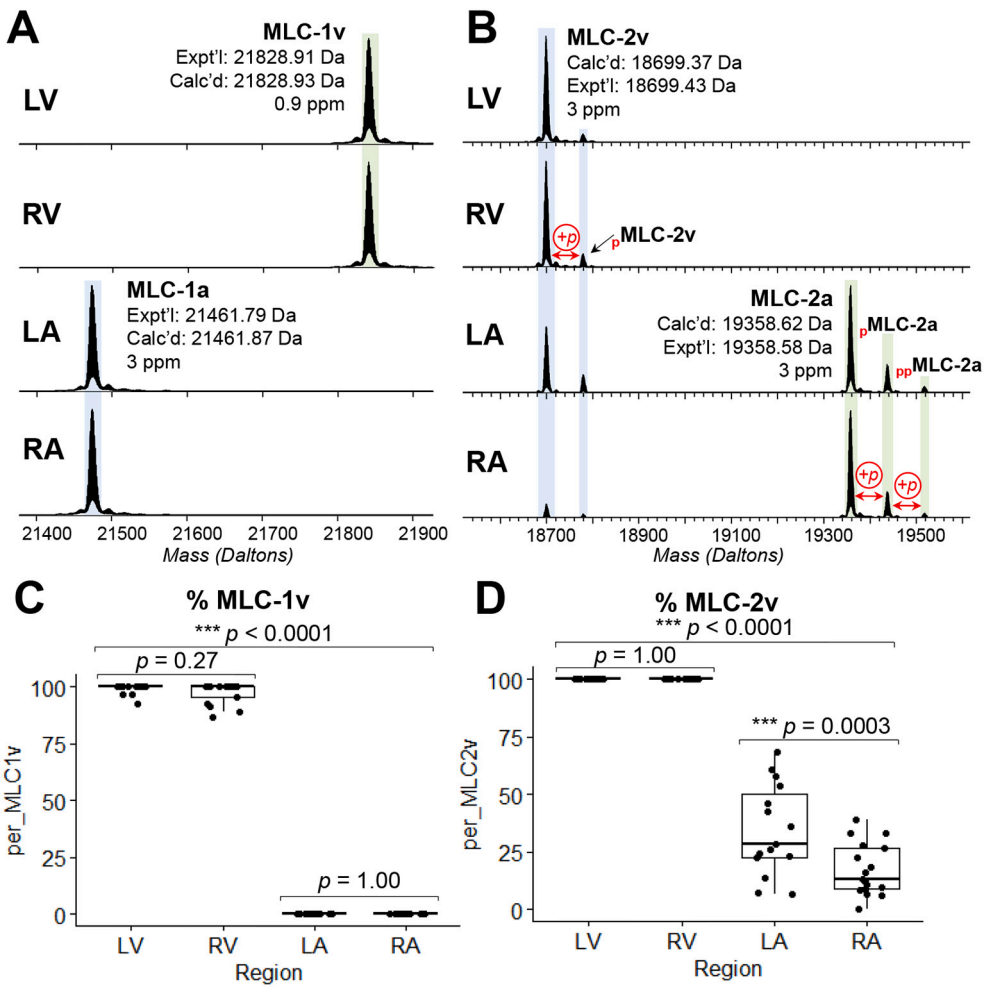

Fig. 1. Top-down MS of MLCs Reveals MLC-1v is Ventricle-specific. A) Deconvoluted spectra showing expression of ventricular and atrial isoforms of myosin light chain 1 (MLC-1). MLC-1v is the dominant isoform in LV and RV tissues and was exclusively detected in LV and RV. MLC-1a was the only isoform detected in LA and RA tissues. B) Deconvoluted spectra showing ventricular and atrial isoforms of myosin light chain 2 (MLC-2). MLC-2v was consistently detected throughout all four chambers of the human heart. MLC-2v was the dominant isoform in LV and RV and detected at varying levels in LA and RA. The atrial isoform MLC-2a was detected exclusively in LA and RA. Isotopic resolution was achieved for each of the isoforms and all proteins were identified with high mass accuracy (3 ppm mass error). C) Quantitation of the expression of MLC-1v relative to total MLC-1a + MLC-1v in LV, RV, LA, and RA (n = 17 donors). Statistically-significant differences across the four chambers were determined by one-way ANOVA followed by Tukey's HSD *post hoc* test for pairwise comparisons ($p \leq 0.05$). One-way ANOVA resulted in overall p value of 2.2e-16 (Table S3). Results of pairwise comparisons are reported on the plot and are notated with an asterisk (*): *$p \leq 0.05$, **$p < 0.01$, and ***$p < 0.001$; no statistical significance if $p > 0.05$. D) Quantitation of the expression of MLC-2v relative to total MLC-2a + MLC-2 V in LV, RV, LA, and RA (n = 17 donors). Statistically-significant differences across the four chambers were determined by one-way ANOVA followed by Tukey's HSD *post hoc* test for pairwise comparisons ($p \leq 0.05$). One-way ANOVA resulted in overall p value of 2.0e-16 (Table S3). Results of pairwise comparisons are reported on the plot and are notated with an asterisk (*): *$p \leq 0.05$, **$p < 0.01$, and ***$p < 0.001$; no statistical significance if $p > 0.05$.

after the addition of HPO_3 (Fig. S18C, D). Due to considerable sequence heterogeneity between MLC-2v and MLC-2a [42], the observed fragment ions overwhelmingly indicate the presence of MLC-2v in the atrial chambers and do not match with a truncated or alternatively-spliced MLC-2a isoform. LC-MS/MS revealed key fragment ions matching to the reported sequence of MLC-2a, such as the y_{25} ion shown across left and right atrial tissues (Fig. S17B). In sum, 37 b and 12 y ions were matched to the MLC-2a sequence within ≤10 ppm mass error, resulting in 61% sequence coverage (Fig. S196). Sequence alignment of MLC-2v and MLC-2a revealed 62.1% sequence similarity between isoforms (Fig. S10B).

Quantification of MLC-2 isoforms revealed significant differences of MLC-2v expression across the four cardiac chambers. In LV and RV, MLC-2v remained at 100% of total signal. MLC-2v content ranged widely in atrial tissues, from 6 to 68% in LA and 0–39% in RA, averaging 34 ± 5.1% MLC-2v in LA and 17 ± 2.7% in RA. MLC-2a was not detected above baseline noise in LV and RV, as shown by close examination of each raw mass spectrum (Fig. S14). MLC-2v expression across the four chambers was significant by one-way ANOVA (p = 2.0e-16) (Fig. 1D). Pairwise comparisons between LV, RV, LA, and RA revealed significant differences between ventricles and atria (all pairwise comparisons $p <$ 0.0001 by Tukey HSD). The % MLC-2v was also statistically significant laterally, between LA and RA ($p = 0.0003$).

No chamber-related differences in relative phosphorylation (mol P_i/mol protein, or P_{total}) of MLC-2 isoforms were detected. The relative phosphorylation (P_{total}) of MLC-2v is 0.15 ± 0.02 in LV and 0.13 ± 0.02 in RV, 0.19 ± 0.03 in LA, and 0.16 ± 0.03 in RA. These values did not yield a significant difference across the four chambers ($p = 0.48$) when compared by one-way ANOVA (Fig. S15C). Similarly, a comparison of the relative phosphorylation (P_{total}) of MLC-2a between the left and right atria (0.25 ± 0.03 in LA and 0.22 ± 0.03 in RA) was not significantly different ($p = 0.52$ by Student t-test).

3.4. Atrial-specific deamidation of MLC-2v localized to N13 by MS/MS

Top-down MS-based proteomics identified and localized an atrial-specific deamidation of human MLC-2v. A difference of +0.98 Da was found in the measured monoisotopic masses of MLC-2v in atrial tissues compared to ventricular tissue (Fig. 2A). N-terminal fragment ions produced by CID MS/MS revealed a + 0.98 Da mass shift near the N-terminus of the protein. This phenomenon was observed in all N-terminal fragments produced by CID MS/MS in atrial tissue, including the shortest fragment b_{15} (Fig. 2B). Putative PTMs matching the observed mass shift are deamidation of asparagine [43] or citrullination of arginine [44]. Since both asparagine and arginine residues are in the first 15 aa residues of MLC-2v sequence, fragmentation closer to the N-terminus was needed to localize and identify the PTM. However, the CID spectra contained no N-terminal fragments shorter than b_{15}, possibly due to the

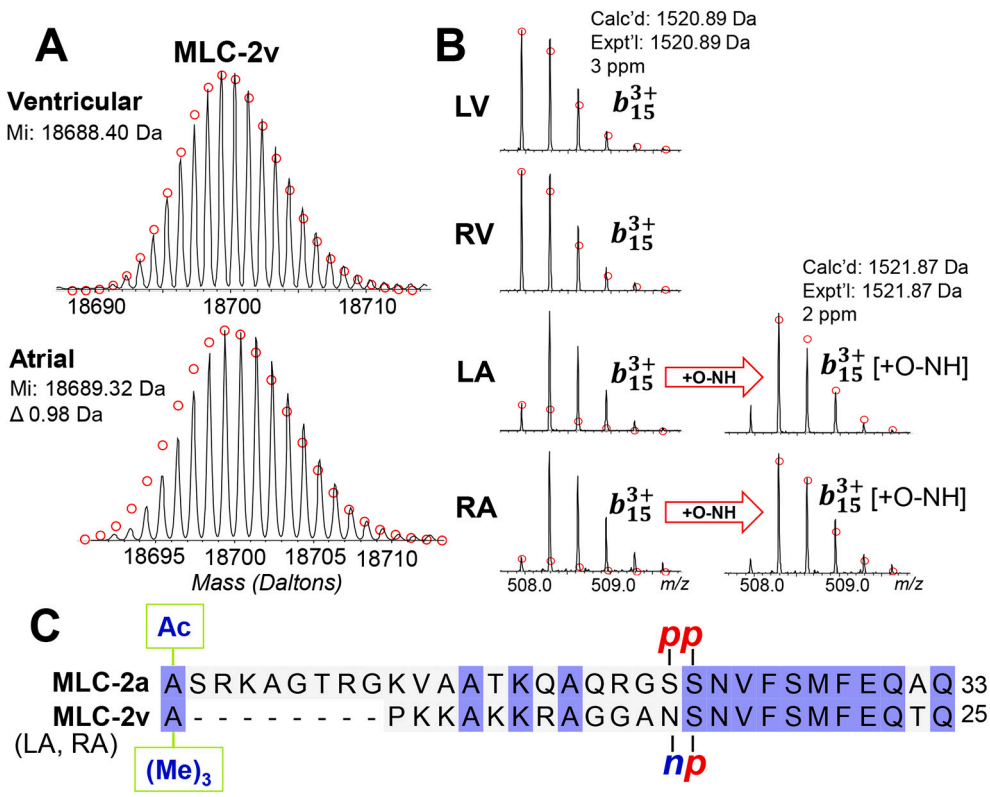

Fig. 2. Atrial-Specific Deamidation of MLC-2v Localized to N13 by MS/MS. A) Deconvoluted spectra of MLC-2v showing a difference of 0.98 Da in monoisotopic mass detected between ventricular and atrial tissues. B) Fragment ion spectra of b_{15}, the smallest N-terminal fragment of MLC-2v observed by CID MS/MS. Deamidation (+0.984 Da) was added to the theoretical mass of ion b_{15} and the resulting theoretical isotopic distribution was fitted in LA and RA. C) Sequence alignment of the first 33 residues of MLC-2a (*MYL7*, Q01449–1, above) and 25 residues of MLC-2v (*MYL2*, P10916–1, below) with deamidation indicated at residue N13. Sequence alignment shows site of phosphorylation at Ser22 in MLC-2a matches with site of deamidation at N13 in MLC-2v sequence. Other PTMs indicated are summarized in Table S2.

basic nature of amino acid residues, which may have inhibited fragmentation by CID by conferring resonance-induced stability to the peptide backbone [45].

To further localize the putative modification, we utilized ETD to generate shorter N-terminal fragments. ETD revealed shorter N-terminal fragments including c_7, c_8, c_9, and c_{12} that matched well to calculated isotopic distribution of MLC-2v sequence and displayed comparable intensities to the same fragment ions observed in LV and RV (Fig. S20A). This result eliminates the possibility of citrullination at the Arg8 residue, indicating the PTM is located between residues aa[12–15]. A c_{14} ion showed a reduction of monoisotopic intensity and aligned to the MLC-2v aa[1–14] when accounting for deamidation [+O-NH] (Fig. S20B), indicating the PTM was located between aa[12–14]. We assigned the putative PTM corresponding to +0.98 Da as deamidation located at Asp13 based on the identity of isolated residues and mass shift. We conclude there is a mixture of deamidated and unmodified MLC-2v proteoform species in the atrial tissues due to the observed overlapping isotopic envelopes of N-terminal fragment ions. Since this PTM was only detected in LA and RA (LV or RV had normal isotopomer distribution matching the predicted N-terminal sequence), the observed atrial deamidation is not an artefactual or preparation-based modification, but one with potential biological relevance.

3.5. Sex differences in MLC proteoforms

Next, we sought to investigate whether sex differences could be correlated to the variability in MLC proteoform patterns given the sex-balanced cohort of non-failing donor hearts (Fig. 3, Table S4). Strikingly, the relative phosphorylation of both MLC-2v and MLC-2a was consistently lower in the female donor hearts as compared to male donor hearts. In LV, the relative phosphorylation (P_{total}) of MLC-2v was 0.20 ± 0.03 in male donor hearts *vs.* 0.10 ± 0.01 in female donor hearts, corresponding to a two-fold change (Fig. 3A) with statistical significance (p = 8.8E-03, two-tailed Student *t*-test; Table S4. Similarly, MLC-2v relative phosphorylation (P_{total}) measured in RV was 0.17 ± 0.03 in male donor hearts *vs* 0.10 ± 0.01 in female donors, corresponding to 1.7-fold change (p = 0.046, Fig. 3B). In LA, MLC-2v relative phosphorylation (P_{total}) increased by 2.2-fold in males (0.26 ± 0.05) compared to females (0.12 ± 0.02, p = 0.036, Fig. 3C). In RA tissue, MLC-2v relative phosphorylation (P_{total}) was 0.21 ± 0.05 in males *vs* 0.12 ± 0.05 in females, with 1.7-fold change but without statistical significance (p = 0.16, Fig. 3D). Representative deconvoluted mass spectra between age-matched males and females demonstrate higher relative abundance of *p*MLC-2v in male LV tissues (Fig. 3E) and male LA tissues (Fig. 3F).

The relative phosphorylation (P_{total}) of MLC-2a in LA is 0.34 ± 0.05 in males and 0.16 ± 0.02 in females, corresponding to a 2.1-fold change in the male LA tissues (p = 0.0098, Fig. 3G). MLC-2a relative phosphorylation (P_{total}) in RA increased by 1.8-fold in male donor hearts (0.28 ± 0.05) compared to female donor hearts (0.16 ± 0.02, p = 0.047, Fig. 3H). Deconvoluted mass spectra between age-matched males and females reflects higher relative abundance of *p*MLC-2a and *pp*MLC-2a in LA tissues from male donor hearts compared to female donor hearts (Fig. 3I).

4. Discussion

In this study, we characterized the spatial distribution of MLC isoforms across ventricular and atrial tissue of adult non-failing human hearts. To identify and quantify the MLC isoforms in different chambers from human cardiac tissue, we used top-down MS-based proteomics to enable a "bird's eye view" of the intact MLCs, revealing unique patterns of isoform expression and PTMs across the four chambers of the human heart.

4.1. MLC-1v, but not MLC-2v, is ventricle-specific in human hearts

In the mature heart, MLC atrial and ventricular isoforms are widely considered to be chamber-specific [6,7], but in this study, top-down MS-based proteomics uncovers unambiguous evidence of expression of MLC-2v in human atrial tissues. Fig. 1 shows the detection and

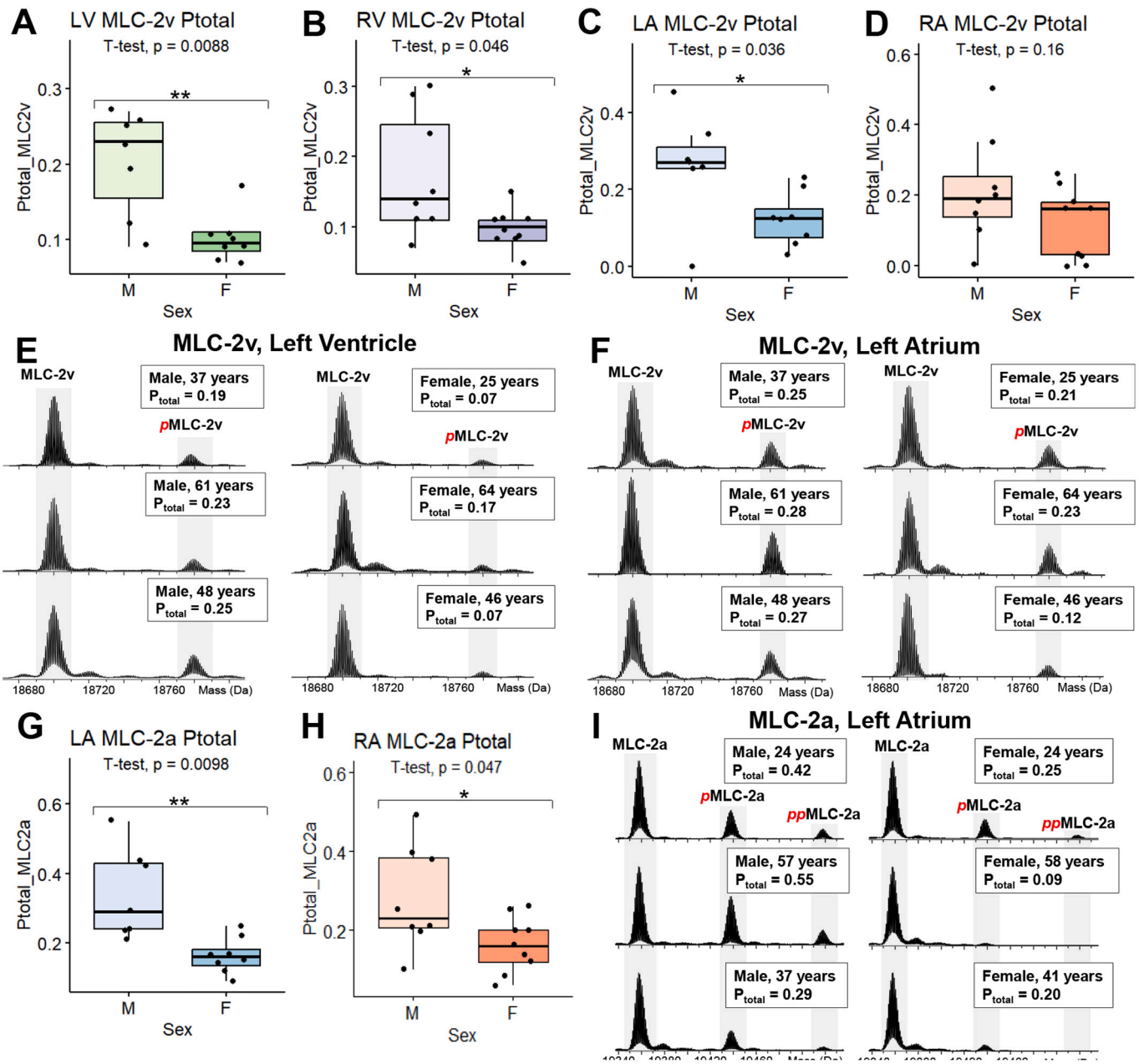

Fig. 3. Sex Differences in MLC-2 Proteoforms. A-D) Comparison of relative phosphorylation (P_{total}) of MLC-2v between M and F donors in A) Left Ventricular (LV) tissues, B) Right Ventricular (RV) tissues, C) Left Atrial (LA) tissues, and D) Right Atrial (RA) Tissues. Results of statistical analysis are summarized in Table S4. Levels of statistical significance are notated with an asterisk (*): $*p \leq 0.05$, $**p < 0.01$, and $***p < 0.001$; no statistical significance if $p > 0.05$. E) Representative deconvoluted mass spectra of MLC-2v expressed in LV and F) LA from male and female donors. Ages at time of donation are listed. MLC-2 and *p*MLC-2v are highlighted, and the measured P_{total} ratio for each mass spectrum is reported. G) Comparison of P_{total} values of MLC-2a between M and F donors in LA tissues and H) RA tissues. I) Representative deconvoluted mass spectra of MLC-2a expressed in LA from male and female donors. Ages at time of donation are listed.

quantification of MLC isoforms across LV, RV, LA, and RA. We found MLC-1v but not MLC-2v exhibits ventricular-restricted expression. Peaks matching molecular masses of MLC-2v and *p*MLC-2v were identified in atrial tissue. Strikingly, MLC-2v was detected in the atria of every heart from all 17 donors with no cardiac diseases. The %MLC-2v of total MLC-2 content was quantitated and deemed statistically significant by one-way ANOVA, with significant differences between ventricular and atrial samples and a lateral difference between LA and RA.

An analysis of myofilament isoform and proteoform expression across the four cardiac chambers of 3 month old Yorkshire domestic pigs was previously performed by our lab [24]. This previous study revealed chamber-specific expression of the atrial and ventricular isoforms of MLC-1 and -2. Importantly, we did not observe expression of MLC-2v in atrial tissue from pig as we did in the human tissue analyzed in this study. This underscores the critical importance of direct interrogation of human samples despite the high similarity between large animals and human hearts [25].

MLC-1a and -1v have well-established functional differences in both actin-myosin tethering and cross-bridge cycling kinetics [3]. Ventricular expression of MLC-1a has been found under states of stress such as cardiomyopathy [46]. It is possible MLC-2v functions as a similar adaptive isoform switch during a state of cardiac stress similarly to MLC-1. MLC-2v has been detected in atrial tissue in previous studies of pressure overload in both humans [47] and rats [48]. Interestingly, MLC-2v was also found in atria of adult spontaneously hypertensive rats without induced pressure overload, suggesting the expression of the

ventricular isoform in atrial tissue was the result of a predetermined phenotype rather than a direct response to pressure overload [48]. Functionally, ventricular and atrial isoforms of MLC-2 have been shown to affect the morphogenesis and cross bridge cycling of the myocardium [6]. In transgenic mice, replacement of MLC-2a by -2v in atria has shown enhanced contractile generation and calcium sensitivity similar to the ventricular cardiomyocyte controls [49,50]. A nuanced assessment of specific isoform influence on either atrial or ventricular function, and the regulation of their differential expression in healthy and diseased states, remains to be explored.

Previously, bottom-up shotgun proteomics was employed to provide a region and cell-type resolved quantitative landscape of the human heart proteome by Doll et al. [51] MLC-2v (*MLY2*) and MLC-1v (*MLY3*) were recovered in this bottom-up study and still considered as a known markers for ventricles [51]. Note that missing values were imputed on the basis of normal distribution in this report which may affect the quantitation results. In a more recent bottom-up paper by Linscheid *et al*, cardiac tissues from each chamber of human, pig, and other model organisms were analyzed [25]. Similarly in this study, values were imputed with standard settings in Perseus from a left-shifted normal distribution. Overall, the stochastic nature of data collection in shotgun proteomics experiments leads to significant missingness in the data, leading to implementation of post-processing procedures such as imputation [52,53]. Since "bottom-up" proteomics analyzes peptides resulted from digestion, inferring measured peptides back to protein content in the original sample [34]. As a result, there are intrinsic limitations in the protein quantitation in the bottom-up proteomics due to this protein inference problem [27,54]. Important biological discoveries may be missed by assuming that all peptides from a protein-coding sequence are representative of the same protein [33]. In contrast, top-down proteomics analyzes proteins directly without digestion thus could provide more accurate identification and quantitation of isoforms together with PTMs [27–31,34]. Here this study provides unambiguous identification and quantitation of all MLC isoforms across the four chambers of non-failing human donor hearts.

4.2. Identification of atrial-specific MLC-2v deamidation on Asn13

We detected a small mass difference of <1 Da in MLC-2v in the atrial tissues compared to the ventricles in each human heart analyzed. Fig. 2 details the localization and identification of this PTM using a combination of fragmentation methods (CID and ETD). Deamidation of MLC-2v from non-failing human cardiac tissue has been previously reported by analysis of enriched tryptic peptides by tandem MS. [55] For the first time, we have localized deamidation to the Asn13 residue in human MLC-2v using a combination of ETD and CID. This site is consistent with a previous assignment of Asn13 as the site of deamidation of MLC-2v in rabbit myocardium [56] and in non-human primate skeletal muscle (MLC-2 s isoform) [57].

The site of deamidation is adjacent to the regulatory phosphorylation site Ser14. The additional negative charge imparted by deamidation [58] adjacent to the site of phosphorylation mimics the pattern of bis-phosphorylation of MLC-2a at sites Ser22/23 (Fig. 2C). Atrial-specific deamidation of MLC-2v may have functional implications relating to cardiac force generation in the atrial chambers. Phosphorylation induces a conformational change in MLC-2 [55], and the addition of a second negative charge may serve to heighten calcium sensitivity and induce further conformational change to the protein. Further investigation to determine the functional consequences of atrial-specific deamidation in human MLC-2v may help elucidate the role of partial replacement from MLC-2a to MLC-2v in the atria.

4.3. Sex-differences in the phosphorylation of MLC-2

Given our sex-balanced donor cohort (9 females and 8 males), we investigated whether sex differences could be correlated to changes in MLC expression (Fig. 3). Notably, we found the relative phosphorylation (P_{total}) of both MLC-2 atrial and ventricular isoforms was consistently higher in male donor hearts compared to female donor hearts. MLC-2 is primarily phosphorylated by a cardiac-specific Ca^{2+}/calmodulin-activated myosin light chain kinase (MLCK) and de-phosphorylated by myosin light chain phosphatases [58–60]. Functionally, phosphorylation of MLC-2 increases the calcium sensitivity of the sarcomere through modulating cross-bridge cycling kinetics and steric interaction with myosin binding protein C (MyBP-C) [58,61]. A previous study in female C57BL/6 J mice suggested female sex hormones may influence myofilament calcium sensitivity and phosphorylation of myofilament proteins including MyBP-C, resulting in overall decreased calcium sensitivity at certain times in the estrous cycle [62]. Additionally, a study in adult Sprague–Dawley rats reported a 32% decrease ($p = 0.011$) in MLC-2v phosphorylation in females by 2D gel electrophoresis [63]. Overall, the findings from this study provide the direct evidence of sex-based difference in cardiac myofilament PTMs.

4.4. Implications for 'chamber-specific' in vitro hPSC-CM models

As maturation strategies of cultured human pluripotent stem cells (hPSC-CMs) advance [64,65], an understanding of sarcomeric isoform and proteoform distribution in healthy adult human cardiac tissue is a useful tool to benchmark against hPSC-CM matured phenotypes *in vitro*. While hPSC-CMs remain phenotypically immature, the present results detailing chamber-specific MLC isoform expression can inform efforts to faithfully recapitulate endogenous adult CMs, including atrial- and ventricular-specific populations. For example, atrial-exclusive populations of hPSC-CMs have been used to model the pathophysiology of atrial fibrillation and its effects on contractile function [66,67]. While the absence of MLC-2v expression is often used to verify atrial-like hPSC-CMs [66], the present results indicate MLC-2v can be found alongside MLC-2a in human adult atrial tissue in the majority our human cohort (35 of 36 atrial tissues). For applications seeking to closely resemble adult atrial cardiomyocyte physiology, the presence, or absence, of MLC-2v may be an important consideration since there are known isoform-specific effects on contractile performance form both animal and human disease models [49,68]. MLC-2v is also a commonly-used marker of ventricular specification in hPSC-CM cultures, with the assumption that its presence is indicative of successful ventricular cardiomyocyte differentiation [10,69], but the present study identifies MLC-2v in adult atrial cardiomyocytes suggesting caution in using this protein marker alone to identify ventricular cardiomyocytes. In contrast, MLC-1a and MLC1-v have been largely overlooked in the chamber-specific characterization of hPSC-CMs, but the data presented here suggest that in adult heart, these proteins provide a highly specific chamber expression pattern. Nevertheless, robust characterization of hPSC-CM chamber specificity based on MLC expression requires consideration of the changes in isoform expression during development [11], and the present study provides only a snapshot of adult heart expression patterns.

5. Conclusion

In this study, we characterized the chamber-specific distribution of MLC isoforms in adult non-failing human hearts ($n = 17$) using top-down MS-based proteomics. MLC atrial and ventricular isoforms are widely considered to be chamber-specific [6,7], but top-down MS-based proteomics has uncovered evidence of expression of MLC-2v in human atrial tissues. Top-down proteomics enables an unbiased analysis of isoform distribution in the human heart by directly analyzing intact proteins to reveal PTMs. Here, we found MLC-1v but not MLC-2v exhibits ventricular-restricted expression. We confirmed the protein sequence of MLC-2v in the atria using high resolution top-down MS/MS and detected a deamidated species of MLC-2v exclusive to atrial tissue. The modification was localized to the N13 residue in MLC-2v. Such "bird's eye view" of the proteome by top-down proteomics can unveil

previously unattainable knowledge of isoform distribution in the heart.

Supplementary data to this article can be found online at https://doi.org/10.1016/j.yjmcc.2023.06.003.

Declaration of Competing Interest

T.J. Kamp is a consultant for Fujifilm Cellular Dynamics Incorporated.

Data availability

Raw data are available in the MassIVE repository with identifier MSV000091143.

Acknowledgements

We are grateful to the donors and their families for their generous donation of tissue. We thank those who assisted with cardiac tissue collection and dissection, especially Tim Zhou, MD. We thank James Anderson and Carrie Sparks at the University of Wisconsin Organ and Tissue Donation for coordination of donor heart collection. Financial support was provided by National Institutes of Health (NIH) R01 HL096971 (Y.G.) and R01 HL109810 (Y.G.). Y.G. also acknowledges R01 GM117058, R01 GM125085, and S10 OD018475. S.P.P. acknowledges support from R01 HL148059-01. K.J.R acknowledges the National Science Foundation Graduate Research Fellowship Program under Grant No. DGE-1747503 and the Graduate School and the Office of the Vice Chancellor for Research and Graduate Education at the University of Wisconsin-Madison, funded by Wisconsin Alumni Research Foundation. D.S.R. acknowledges support from the American Heart Association Predoctoral Fellowship Grant No. 832615/David S. Roberts/2021. T.J. A. acknowledges support from the NIH Training Grant T32 GM008688. E.A.C. acknowledges support from the NIH Chemistry-Biology Interface Training Program NIH T32GM008505. W.G. and Z.G. acknowledge funding from the NIH NHBLI HL148733 and the American Heart Association Foundation 19TPA3480072. J.C.R. acknowledges support from R01 HL139883. Any opinions, findings, and conclusions or recommendations expressed in this material are those of the authors and do not necessarily reflect the views of the National Science Foundation.

References

[1] H.M. Warrick, J.A. Spudich, Myosin structure and function in cell motility, Annu. Rev. Cell Biol. 3 (1) (1987) 379–421, https://doi.org/10.1146/annurev.cb.03.110187.002115 (acccessed 2023/01/12).

[2] R. Craig, J.L. Woodhead, Structure and function of myosin filaments, Curr. Opin. Struct. Biol. 16 (2) (2006) 204–212, https://doi.org/10.1016/j.sbi.2006.03.006.

[3] I. Morano, Tuning the human heart molecular motors by myosin light chains, J. Mol. Med. 77 (7) (1999) 544–555, https://doi.org/10.1007/s001099900031.

[4] S.M. Heissler, J.R. Sellers, Myosin light chains: teaching old dogs new tricks, BioArchitecture 4 (6) (2014) 169–188, https://doi.org/10.1080/19490992.2015.1054092.

[5] Y.H. Sitbon, S. Yadav, K. Kazmierczak, D. Szczesna-Cordary, Insights into myosin regulatory and essential light chains: a focus on their roles in cardiac and skeletal muscle function, development and disease, J. Muscle Res. Cell Motil. 41 (4) (2020) 313–327, https://doi.org/10.1007/s10974-019-09517-x.

[6] F. Sheikh, R.C. Lyon, J. Chen, Functions of myosin light chain-2 (MYL2) in cardiac muscle and disease, Gene 569 (1) (2015) 14–20, https://doi.org/10.1016/j.gene.2015.06.027.

[7] J. England, S. Loughna, Heavy and light roles: myosin in the morphogenesis of the heart, Cell. Mol. Life Sci. 70 (7) (2013) 1221–1239, https://doi.org/10.1007/s00018-012-1131-1.

[8] T.X. O'Brien, K.J. Lee, K.R. Chien, Positional specification of ventricular myosin light chain 2 expression in the primitive murine heart tube, Proc. Natl. Acad. Sci. 90 (11) (1993) 5157–5161, https://doi.org/10.1073/pnas.90.11.5157 (accessed 2022/12/27).

[9] S.W. Kubalak, W.C. Miller-Hance, T.X. O'Brien, E. Dyson, K.R. Chien, Chamber specification of atrial myosin light chain-2 expression precedes septation during murine cardiogenesis, J. Biol. Chem. 269 (24) (1994) 16961–16970, https://doi.org/10.1016/S0021-9258(19)89483-8.

[10] A. Bizy, G. Guerrero-Serna, B. Hu, D. Ponce-Balbuena, B.C. Willis, M. Zarzoso, R. J. Ramirez, M.F. Sener, L.V. Mundada, M. Klos, et al., Myosin light chain 2-based selection of human iPSC-derived early ventricular cardiac myocytes, Stem Cell Res. 11 (3) (2013) 1335–1347, https://doi.org/10.1016/j.scr.2013.09.003.

[11] Chuva de Sousa, S.M. Lopes, R.J. Hassink, A. Feijen, M.A. van Rooijen, P. A. Doevendans, L. Tertoolen, A. Brutel de la Rivière, C.L. Mummery, Patterning the heart, a template for human cardiomyocyte development, Dev. Dyn. 235 (7) (2006) 1994–2002, https://doi.org/10.1002/dvdy.20830 (acccessed 2022/11/15).

[12] P. Camacho, H. Fan, Z. Liu, J. He, i.-Q., Small mammalian animal models of heart disease, Am. J. Cardiovasc. Dis. 6 (3) (2016) 70–80.

[13] V. Kooij, V. Venkatraman, J. Tra, J.A. Kirk, J. Rowell, A. Blice-Baum, A. Cammarato, J.E. Van Eyk, Sizing up models of heart failure: proteomics from flies to humans, Proteomics – Clin. Appl. 8 (9–10) (2014) 653–664, https://doi.org/10.1002/prca.201300123 (acccessed 2023/03/24).

[14] N. Milani-Nejad, P.M.L. Janssen, Small and large animal models in cardiac contraction research: advantages and disadvantages, Pharmacol. Ther. 141 (3) (2014) 235–249, https://doi.org/10.1016/j.pharmthera.2013.10.007.

[15] H.G. Tsang, N.A. Rashdan, C.B.A. Whitelaw, B.M. Corcoran, K.M. Summers, V. E. MacRae, Large animal models of cardiovascular disease, Cell Biochem. Funct. 34 (3) (2016) 113–132, https://doi.org/10.1002/cbf.3173 (acccessed 2023/03/24).

[16] S.R. Houser, K.B. Margulies, A.M. Murphy, F.G. Spinale, G.S. Francis, S.D. Prabhu, H.A. Rockman, D.A. Kass, J.D. Molkentin, M.A. Sussman, et al., Animal models of heart failure, Circ. Res. 111 (1) (2012) 131–150, https://doi.org/10.1161/RES.0b013e3182582523 (acccessed 2023/03/24).

[17] J. van der Velden, F.W. Asselbergs, J. Bakkers, S. Batkai, L. Bertrand, C.R. Bezzina, I. Bot, B.J.J.M. Brundel, L. Carrier, S. Chamuleau, et al., Animal models and animal-free innovations for cardiovascular research: current status and routes to be explored. Consensus document of the ESC working group on myocardial function and the ESC working group on cellular biology of the heart, Cardiovasc. Res. 118 (15) (2022) 3016–3051, https://doi.org/10.1093/cvr/cvab370 (acccessed 3/24/2023).

[18] N. Velayutham, K.E. Yutzey, Porcine models of heart regeneration, in: Journal of Cardiovascular Development and Disease vol. 9, 2022.

[19] L. Ye, Y.-H. Chang, Q. Xiong, P. Zhang, L. Zhang, P. Somasundaram, M. Lepley, C. Swingen, L. Su, Jacqueline S. Wendel, et al., Cardiac repair in a porcine model of acute myocardial infarction with human induced pluripotent stem cell-derived cardiovascular cells, Cell Stem Cell 15 (6) (2014) 750–761, https://doi.org/10.1016/j.stem.2014.11.009.

[20] N. Hamdani, M. de Waard, A.E. Messer, N.M. Boontje, V. Kooij, S. van Dijk, A. Versteilen, R. Lamberts, D. Merkus, C. dos Remedios, et al., Myofilament dysfunction in cardiac disease from mice to men, J. Muscle Res. Cell Motil. 29 (6–8) (2008) 189–201.

[21] J. Zhang, X. Dong, T.A. Hacker, Y. Ge, Deciphering modifications in swine cardiac troponin I by top-down high-resolution tandem mass spectrometry, J. Am. Soc. Mass Spectrom. 21 (6) (2010) 940–948, https://doi.org/10.1016/j.jasms.2010.02.005.

[22] Y. Peng, Z.R. Gregorich, S.G. Valeja, H. Zhang, W. Cai, Y.-C. Chen, H. Guner, A. J. Chen, D.J. Schwahn, T.A. Hacker, et al., Top-down proteomics reveals concerted reductions in myofilament and Z-disc protein phosphorylation after acute myocardial infarction, Mol. Cell. Proteomics 13 (10) (2014) 2752, https://doi.org/10.1074/mcp.M114.040675.

[23] E.A. Chapman, T.J. Aballo, J.A. Melby, T. Zhou, S.J. Price, K.J. Rossler, I. Lei, P. C. Tang, Y. Ge, Defining the sarcomeric proteoform landscape in ischemic cardiomyopathy by top-down proteomics, J. Proteome Res. 22 (3) (2023) 931–941, https://doi.org/10.1021/acs.jproteome.2c00729.

[24] Z.R. Gregorich, Y. Peng, N.M. Lane, J.J. Wolff, S. Wang, W. Guo, H. Guner, J. Doop, T.A. Hacker, Y. Ge, Comprehensive assessment of chamber-specific and transmural heterogeneity in myofilament protein phosphorylation by top-down mass spectrometry, J. Mol. Cell. Cardiol. 87 (2015) 102–112.

[25] N. Linscheid, A. Santos, P.C. Poulsen, R.W. Mills, K. Calloe, U. Leurs, J.Z. Ye, C. Stolte, M.B. Thomsen, B.H. Bentzen, et al., Quantitative proteome comparison of human hearts with those of model organisms, PLoS Biol. 19 (4) (2021), e3001144, https://doi.org/10.1371/journal.pbio.3001144.

[26] L.M. Smith, N.L. Kelleher, Consortium for Top Down, P, Proteoform: a single term describing protein complexity, Nat. Methods 10 (3) (2013) 186–187, https://doi.org/10.1038/nmeth.2369.

[27] B. Chen, K.A. Brown, Z. Lin, Y. Ge, Top-down proteomics: ready for prime time? Anal. Chem. 90 (1) (2018) 110–127, https://doi.org/10.1021/acs.analchem.7b04747.

[28] K.A. Brown, J.A. Melby, D.S. Roberts, Y. Ge, Top-down proteomics: challenges, innovations, and applications in basic and clinical research, Expert Rev. Proteomics 17 (10) (2020) 719–733, https://doi.org/10.1080/14789450.2020.1855982.

[29] W. Cai, T.M. Tucholski, Z.R. Gregorich, Y. Ge, Top-down proteomics: technology advancements and applications to heart diseases, Expert Rev. Proteomics 13 (8) (2016) 717–730, https://doi.org/10.1080/14789450.2016.1209414.

[30] Z.R. Gregorich, Y. Ge, Top-down proteomics in health and disease: challenges and opportunities, Proteomics 14 (10) (2014) 1195–1210, https://doi.org/10.1002/pmic.201300432.

[31] L.M. Smith, N.L. Kelleher, Proteoforms as the next proteomics currency, Science 359 (6380) (2018) 1106–1107, https://doi.org/10.1126/science.aat1884 (acccessed 2023/01/12).

[32] A.I. Nesvizhskii, R. Aebersold, Interpretation of shotgun proteomic data, Mol. Cell. Proteomics 4 (10) (2005) 1419–1440, https://doi.org/10.1074/mcp.R500012-MCP200 (acccessed 2023/04/03).

[33] D.L. Plubell, L. Käll, B.-J. Webb-Robertson, L.M. Bramer, A. Ives, N.L. Kelleher, L. M. Smith, T.J. Montine, C.C. Wu, M.J. MacCoss, Putting humpty dumpty back together again: what does protein quantification mean in bottom-up proteomics?

J. Proteome Res. 21 (4) (2022) 891–898, https://doi.org/10.1021/acs.jproteome.1c00894.
[34] Z.R. Gregorich, Y.-H. Chang, Y. Ge, Proteomics in heart failure: top-down or bottom-up? Pflugers Arch. - Eur. J. Physiol. 466 (6) (2014) 1199–1209, https://doi.org/10.1007/s00424-014-1471-9.
[35] Z.R. Gregorich, W. Cai, Z. Lin, A.J. Chen, Y. Peng, T. Kohmoto, Y. Ge, Distinct sequences and post-translational modifications in cardiac atrial and ventricular myosin light chains revealed by top-down mass spectrometry, J. Mol. Cell. Cardiol. 107 (2017) 13–21, https://doi.org/10.1016/j.yjmcc.2017.04.002.
[36] W. Cai, Z.L. Hite, B. Lyu, Z. Wu, Z. Lin, Z.R. Gregorich, A.E. Messer, S.J. McIlwain, S.B. Marston, T. Kohmoto, et al., Temperature-sensitive sarcomeric protein post-translational modifications revealed by top-down proteomics, J. Mol. Cell. Cardiol. 122 (2018) 11–22, https://doi.org/10.1016/j.yjmcc.2018.07.247.
[37] L.A. Kane, I. Neverova, Eyk Van, J. E. Subfractionation of Heart Tissue, in: F. Vivanco (Ed.), Cardiovascular Proteomics: Methods and Protocols, Humana Press, 2007, pp. 87–90.
[38] T. Tucholski, W. Cai, Z.R. Gregorich, E.F. Bayne, S.D. Mitchell, S.J. McIlwain, W. J. de Lange, M. Wrobbel, H. Karp, Z. Hite, et al., Distinct hypertrophic cardiomyopathy genotypes result in convergent sarcomeric proteoform profiles revealed by top-down proteomics, Proc. Natl. Acad. Sci. (2020), https://doi.org/10.1073/pnas.2006764117, 202006764.
[39] Z. Wu, D.S. Roberts, J.A. Melby, K. Wenger, M. Wetzel, Y. Gu, S.G. Ramanathan, E. F. Bayne, X. Liu, R. Sun, et al., MASH explorer: a universal software environment for top-down proteomics, J. Proteome Res. 19 (9) (2022) 3867–3876, https://doi.org/10.1021/acs.jproteome.0c00469.
[40] L. Wei, Z.R. Gregorich, Z. Lin, W. Cai, Y. Jin, S.H. McKiernan, S. McIlwain, J. M. Aiken, R.L. Moss, G.M. Diffee, et al., Novel sarcopenia-related alterations in sarcomeric protein post-translational modifications (PTMs) in skeletal muscles identified by top-down proteomics *, Mol. Cell. Proteomics 17 (1) (2018) 134–145, https://doi.org/10.1074/mcp.RA117.000124 (acccessed 2022/11/06).
[41] Z. Lin, L. Wei, W. Cai, Y. Zhu, T. Tucholski, S.D. Mitchell, W. Guo, S.P. Ford, G. M. Diffee, Y. Ge, Simultaneous quantification of protein expression and modifications by top-down targeted proteomics: a case of the sarcomeric subproteome, Mol. Cell. Proteomics 18 (3) (2019) 594–605.
[42] J. Walklate, C. Ferrantini, C.A. Johnson, C. Tesi, C. Poggesi, M.A. Geeves, Alpha and beta myosin isoforms and human atrial and ventricular contraction, Cell. Mol. Life Sci. 78 (23) (2021) 7309–7337, https://doi.org/10.1007/s00018-021-03971-y.
[43] Y. Jin, Y. Yi, B. Yeung, Mass spectrometric analysis of protein deamidation – a focus on top-down and middle-down mass spectrometry, Methods (2020), https://doi.org/10.1016/j.ymeth.2020.08.002.
[44] R. Vitorino, S. Guedes, C. Vitorino, R. Ferreira, F. Amado, J.E. Van Eyk, Elucidating Citrullination by mass spectrometry and its role in disease pathogenesis, J. Proteome Res. 20 (1) (2021) 38–48, https://doi.org/10.1021/acs.jproteome.0c00474.
[45] D.L. Tabb, Y. Huang, V.H. Wysocki, J.R. Yates, Influence of basic residue content on fragment ion peak intensities in low-energy collision-induced dissociation spectra of peptides, Anal. Chem. 76 (5) (2004) 1243–1248, https://doi.org/10.1021/ac0351163.
[46] Adam M. Jacques, N. Briceno, A.E. Messer, C.E. Gallon, S. Jalilzadeh, E. Garcia, G. Kikonda-Kanda, J. Goddard, S.E. Harding, H. Watkins, et al., The molecular phenotype of human cardiac myosin associated with hypertrophic obstructive cardiomyopathy, Cardiovasc. Res. 79 (3) (2008) 481–491.
[47] P. Cummins, Transitions in human atrial and ventricular myosin light-chain isoenzymes in response to cardiac-pressure-overload-induced hypertrophy, Biochem. J. 205 (1) (1982) 195–204, https://doi.org/10.1042/bj2050195 (acccessed 12/28/2022).
[48] C. Kumar, C. Saidapet, P. Delaney, C. Mendola, M.A. Siddiqui, Expression of ventricular-type myosin light chain messenger RNA in spontaneously hypertensive rat atria, Circ. Res. 62 (6) (1988) 1093–1097, https://doi.org/10.1161/01.RES.62.6.1093 (acccessed 2022/12/28).
[49] C.M. Pawloski-Dahm, G. Song, D.L. Kirkpatrick, J. Palermo, J. Gulick, G.W. Dorn, J. Robbins, R.A. Walsh, Effects of total replacement of atrial myosin light Chain-2 with the ventricular isoform in atrial myocytes of transgenic mice, Circulation 97 (15) (1998) 1508–1513, https://doi.org/10.1161/01.CIR.97.15.1508 (acccessed 2022/11/16).
[50] S.H. Buck, P.J. Konyn, J. Palermo, J. Robbins, R.L. Moss, Altered kinetics of contraction of mouse atrial myocytes expressing ventricular myosin regulatory light chain, Am. J. Phys. Heart Circ. Phys. 276 (4) (1999) H1167–H1171, https://doi.org/10.1152/ajpheart.1999.276.4.H1167 (acccessed 2022/12/28).
[51] S. Doll, M. Dreßen, P.E. Geyer, D.N. Itzhak, C. Braun, S.A. Doppler, F. Meier, M.-A. Deutsch, H. Lahm, R. Lange, et al., Region and cell-type resolved quantitative proteomic map of the human heart, Nat. Commun. 8 (2017) 1.
[52] B.-J.M. Webb-Robertson, H.K. Wiberg, M.M. Matzke, J.N. Brown, J. Wang, J. E. McDermott, R.D. Smith, K.D. Rodland, T.O. Metz, J.G. Pounds, et al., Review, evaluation, and discussion of the challenges of missing value imputation for mass spectrometry-based label-free global proteomics, J. Proteome Res. 14 (5) (2015) 1993–2001, https://doi.org/10.1021/pr501138h.
[53] L. Jin, Y. Bi, C. Hu, J. Qu, S. Shen, X. Wang, Y. Tian, A comparative study of evaluating missing value imputation methods in label-free proteomics, Sci. Rep. 11 (1) (2021) 1760, https://doi.org/10.1038/s41598-021-81279-4.
[54] T.K. Toby, L. Fornelli, N.L. Kelleher, Progress in top-down proteomics and the analysis of Proteoforms, Annu. Rev. Anal. Chem. 9 (1) (2016) 499–519, https://doi.org/10.1146/annurev-anchem-071015-041550 (acccessed 2023/04/08).
[55] S.B. Scruggs, R. Reisdorph, M.L. Armstrong, C.M. Warren, N. Reisdorph, R. J. Solaro, P.M. Buttrick, A novel, in-solution separation of endogenous cardiac sarcomeric proteins and identification of distinct charged variants of regulatory light chain, Mol. Cell. Proteomics 9 (9) (2010) 1804–1818, https://doi.org/10.1074/mcp.M110.000075.
[56] M.Y. White, S.J. Cordwell, H.C.K. McCarron, A.S. Tchen, B.D. Hambly, R. W. Jeremy, Modifications of myosin-regulatory light chain correlate with function of stunned myocardium, J. Mol. Cell. Cardiol. 35 (7) (2003) 833–840, https://doi.org/10.1016/S0022-2828(03)00141-X.
[57] Y. Jin, G.M. Diffee, R.J. Colman, R.M. Anderson, Y. Ge, Top-down mass spectrometry of Sarcomeric protein post-translational modifications from non-human primate skeletal muscle, J. Am. Soc. Mass Spectrom. 30 (12) (2019) 2460–2469, https://doi.org/10.1007/s13361-019-02139-0.
[58] S.B. Scruggs, R.J. Solaro, The significance of regulatory light chain phosphorylation in cardiac physiology, Arch. Biochem. Biophys. 510 (2) (2011) 129–134, https://doi.org/10.1016/j.abb.2011.02.013.
[59] A.N. Chang, K.E. Kamm, J.T. Stull, Role of myosin light chain phosphatase in cardiac physiology and pathophysiology, J. Mol. Cell. Cardiol. 101 (2016) 35–43, https://doi.org/10.1016/j.yjmcc.2016.10.004.
[60] P. Ding, J. Huang, P.K. Battiprolu, J.A. Hill, K.E. Kamm, J.T. Stull, Cardiac myosin light chain kinase is necessary for myosin regulatory light chain phosphorylation and cardiac performance in vivo*, J. Biol. Chem. 285 (52) (2010) 40819–40829, https://doi.org/10.1074/jbc.M110.160499 (acccessed 2023/04/05).
[61] M. Ito, R. Okamoto, H. Ito, Y. Zhe, K. Dohi, Regulation of myosin light-chain phosphorylation and its roles in cardiovascular physiology and pathophysiology, Hypertens. Res. 45 (1) (2022) 40–52, https://doi.org/10.1038/s41440-021-00733-y.
[62] J.K. MacDonald, W.G. Pyle, C.J. Reitz, S.E. Howlett, Cardiac contraction, calcium transients, and myofilament calcium sensitivity fluctuate with the estrous cycle in young adult female mice, Am. J. Phys. Heart Circ. Phys. 306 (7) (2014) H938–H953, https://doi.org/10.1152/ajpheart.00730.2013 (acccessed 2023/04/06).
[63] C.J. Lagranha, A. Deschamps, A. Aponte, C. Steenbergen, E. Murphy, Sex differences in the phosphorylation of mitochondrial proteins result in reduced production of reactive oxygen species and cardioprotection in females, Circ. Res. 106 (11) (2010) 1681–1691, https://doi.org/10.1161/CIRCRESAHA.109.213645 (acccessed 2023/04/05).
[64] W. Cai, J. Zhang, W.J. de Lange, Z.R. Gregorich, H. Karp, E.T. Farrell, S.D. Mitchell, T. Tucholski, Z. Lin, M. Biermann, et al., An unbiased proteomics method to assess the maturation of human pluripotent stem cell–derived cardiomyocytes, Circ. Res. 125 (2019) 936–953.
[65] E. Karbassi, A. Fenix, S. Marchiano, N. Muraoka, K. Nakamura, X. Yang, C. E. Murry, Cardiomyocyte maturation: advances in knowledge and implications for regenerative medicine, Nat. Rev. Cardiol. 17 (6) (2020) 341–359, https://doi.org/10.1038/s41569-019-0331-x.
[66] M. Gharanei, S. Shafaattalab, S. Sangha, M. Gunawan, Z. Laksman, L. Hove-Madsen, G.F. Tibbits, Atrial-specific hiPSC-derived cardiomyocytes in drug discovery and disease modeling, Methods 203 (2022) 364–377, https://doi.org/10.1016/j.ymeth.2021.06.009.
[67] P. Benzoni, G. Campostrini, S. Landi, V. Bertini, E. Marchina, M. Iascone, G. Ahlberg, M.S. Olesen, E. Crescini, C. Mora, et al., Human iPSC modelling of a familial form of atrial fibrillation reveals a gain of function of if and ICaL in patient-derived cardiomyocytes, Cardiovasc. Res. 116 (6) (2020) 1147–1160, https://doi.org/10.1093/cvr/cvz217 (acccessed 11/15/2022).
[68] B.M. Palmer, Thick filament proteins and performance in human heart failure, Heart Fail. Rev. 10 (3) (2005) 187–197, https://doi.org/10.1007/s10741-005-5249-1.
[69] O. Chirikian, W.R. Goodyer, E. Dzilic, V. Serpooshan, J.W. Buikema, W. McKeithan, H. Wu, G. Li, S. Lee, M. Merk, et al., CRISPR/Cas9-based targeting of fluorescent reporters to human iPSCs to isolate atrial and ventricular-specific cardiomyocytes, Sci. Rep. 11 (1) (2021) 3026, https://doi.org/10.1038/s41598-021-81860-x.